

MODELLING OF FLUIDIZED BED CHANNELLING USING A TWO-ZONE MODEL

Ivan MACHAČ, Bedřich ŠIŠKA and Miloslav SIMON

Institute of Environmental and Chemical Engineering,
The University of Pardubice, CZ-532-10 Pardubice

This paper deals with the study of the structure of spherical particle beds fluidized with non-Newtonian aqueous polymer solutions in the creeping flow region in a two-dimensional rectangular column. The results confirmed that the bed channelling creates and the bed expansion reduces in fluidization with viscoelastic liquids. A simple two-zone model was used to describe the bed channelling.

Introduction

The fluidization of monodispersed beds of solid particles with liquids is usually considered to be uniform. However, extensive investigations of expansion of beds of solid particles fluidized with different kinds of non-Newtonian liquids performed in our laboratory show that the expansion course depends in a great measure on rheological behaviour of the fluid [1-5]. For the fluidization with viscoelastic (pseudoplastic and simultaneously elastic) polymer solutions in creeping flow region, it has been observed that the fluidization becomes aggregative. The remarkable local particle concentration inhomogeneity gradually creates in the bed up to the state of bed channelling [6]. At the same time, the bed expansion reduces due to that phenomenon.

It has been found that the shapes of expansion curves obtained for fluidization in cylindrical and narrow rectangular (“two-dimensional”) columns are similar [2]. From here, it can be deduced that the structure of beds fluidized in these columns will be similar as well. At the same time, the creation of particle aggregates and bed channelling occurring in the bed is in a “two-dimensional” column conveniently visually observable.

In this paper, the results are presented of examining the effect of the liquid rheological behaviour on the fluidized bed structure and expansion course in the flow of purely viscous and viscoelastic polymer solutions in a narrow rectangular column. The two-zone model was used for describing the fluidized bed channelling observed. The parameters of the two-zone model were evaluated using an image analysis of the video records of the flow through the bed. For visualisation of the liquid flow a method based on the observation of hydrogen bubbles created by electrolysis of water was used.

Two-zone model

The quantities characterizing channelling in a fluidized bed can be evaluated using the two-zone bed model [7]. The fluidized bed is considered to be divided into two zones: one with uniformly dispersed particles with the voidage ε_l and the other consisting of fluid channel (Fig. 1). Then, the mean bed voidage is expressed as

$$\varepsilon = \frac{V_{ch} + (V - V_{ch})\varepsilon_l}{V} = \frac{S_{ch}}{S} + \left(1 - \frac{S_{ch}}{S}\right)\varepsilon_l = f \frac{u}{u_{ch}} + \left(1 - f \frac{u}{u_{ch}}\right)\varepsilon_l \quad (1)$$

where S is the cross-section of the whole bed, S_{ch} is the cross-section of the channels, u is the fluid superficial velocity, u_{ch} is the velocity of the liquid flowing through the channels and

$$f = \frac{S_{ch}u_{ch}}{S u} \quad (2)$$

is the fraction of the liquid volume flow rate flowing through the channels.

If it is supposed that the voidage ε_l is expressed by the Richardson-Zaki type equation

$$\varepsilon_l = \left(\frac{u_l}{F_w u_t}\right)^{\frac{1}{z}}, \quad (3)$$

where u_l is the superficial velocity of the liquid flowing through the particle zone, u_t is the terminal falling velocity of particles, z is the Richardson-Zaki exponent, and F_w is the wall factor, we can derive that

$$f = 1 - \frac{1 - \varepsilon}{1 - \varepsilon_l} \varepsilon_l^z \frac{u_t}{u} F_w \quad (4)$$

The parameters needed for the model evaluation should be determined experimentally.

Experimental

The extensive fluidization experiments were performed in the frame of the doctoral work [8]. Here, with respect to the limited extent of the contribution, only a representative set of experiments is presented.

The particle beds were composed of uniform glass spheres with diameter and density given in Table 1. The test liquids were aqueous solutions of methyl hydroxyethyl cellulose Tylose, hydroxyethyl cellulose Natrosol, and polyacrylamides Praestol and Hercofloc. Flow curves and creep and recovery tests of the liquids were measured on the rotational rheometer RheoStress RS

150 at 23 °C. Terminal velocities u_t of single particles in test liquids were measured in a cylindrical Perspex tube of 40 mm in diameter. A rectangular column made from transparent Perspex sheets was used for fluidization experiments. The column cross-section dimensions were 5 mm x 80 mm and the height of the column was 800 mm. The liquid was pumped by a gear pump. Volumetric liquid flow rate was controlled by changing the pump revolutions.

The hydrogen bubble visualization of the flow was based on the tracing of hydrogen bubbles generated by electrolysis of water under the distributor carrying the bed of particles. Individual stages of fluidized bed expansion were recorded by a video camera and subsequently evaluated by an image analysis. The video sequences recorded by miniDV camera Canon M250i were transferred to the computer through interface IEEE1394 (FireWire). For the image processing and analysis, the freeware programs VirtualDub and ImageJ were used.

The layout of the experimental equipment is shown in Fig. 2. The procedure of measurements and the method of result evaluation are described in detail in the work [8].

Results

Rheological measurements

From the shear stress-shear rate data, the liquid viscosity functions and the parameters η_0 , λ , and m of the Carreau viscosity model

$$\eta = \frac{\eta_0}{\left[1 + (\lambda\dot{\gamma})^2\right]^{\frac{1-m}{2}}} \quad (5)$$

were determined. The liquid relaxation times

$$\lambda_c = \eta_0 J_s(t_0) \quad (6)$$

were evaluated from the creep and recovery tests. The obtained viscosity functions and the examples of creep and recovery tests are shown in Fig. 3 and Fig. 4, respectively. The values of Carreau model parameters are along with liquid densities and relaxation times given in Table 2. All polymer solutions are shear thinning liquids. The values of the relaxation time λ_c give evidence that the solutions of Tylose and Natrosol are very weakly linearly elastic and solutions of Praestol and Hercofloc are strongly linearly elastic liquids.

Expansion and fluidized beds structure

Examples of dependences of the dimensionless velocity $u_B = u/u_t$ on the bed voidage ε (expansion curves) are for fluidization of particles P1 with polymer solution used shown in Fig. 5. Nearly the same course of expansion curves was observed for fluidization of particles P2. It is

evident that the bed expansion reduces with the increasing liquid rate, liquid shear thinning, and elasticity. It is due to the gradual loss of stability of the particulate fluidization; fluidization becomes aggregative, the particle chaining and bed channeling manifests itself. This phenomenon is apparently evoked by the liquid linear elasticity (memory) and enhanced by the creation of liquid streams with lower viscosity due to the liquid shear thinning.

Examples of structures of beds of spherical particle P1 fluidized with liquids differing by their shear thinning and linear elasticity are shown in Fig. 6. During fluidization with shear thinning and slightly elastic solutions of Tylose and Natrosol, only random aggregates of particles and random short channels are created. In the case of fluidization with the strongly shear thinning and elastic solutions of Praestol and Hercofloc, a few stable channels create and the achieved extent of the bed expansion is very small.

Zone model evaluation

For the zone model evaluation, it was necessary to set the following variables: u , u_t , S_{ch}/S , ε , z , and F_w . Values of variables u and ε were obtained from the measurements of bed expansions, values of variables u_t and F_w from the measurements of the terminal falling velocities of particles, and $z = 4.71$ for the spherical particle bed fluidization in creeping flow region [4]. The values of the ratio S_{ch}/S were determined by the image analysis applied to the corresponding fluidization video sequences. Knowing the values of the ratio S_{ch}/S , the values of remaining variables ε , f , u_{ch} , and u_t were calculated using the zone model equations (1), (4), (3), and (2).

Examples of the results obtained from the zone model are for individual systems tested shown in Figs. 7 – 10. The results show the analogous course of fluidization by liquids of comparable rheological properties. During fluidization of particles P1 and P2 with the strong pseudoplastic and linearly elastic polymer solutions Praestol and Hercofloc, the fraction of the liquid volume flowing through the channels $f > 0.85$ and the ratio $u_{ch}/u > 4.4$. For fluidization with polymer solutions of Tylose and Natrosol, which exhibit only weak linear elasticity, the values of the fraction f and the ratio u_{ch}/u are lower than those obtained for the solutions of Praestol and Hercofloc. This is in accordance with the observed lower degree of bed channelling. The velocities u_{ch} calculated using the zone model have been compared with those determined from the visualisation experiments when the velocity of hydrogen bubbles carried by the liquid flowing in the channels was measured. The maximal relative deviation between calculated and experimental values of u_{ch}/u was 13.2%, which documents applicability of the two-zone model to description of fluidized beds channeling.

Conclusions

The expansion of spherical particle beds with liquids of different rheological behavior in rectangular columns was investigated by means of a flow visualization technique and image analysis of fluidized bed video records.

It has been documented that the state of particulate fluidization, observed in fluidization with Newtonian liquids, changes to aggregative one up to channel creation in the case of fluidization with viscoelastic solutions of polymers. The fluidized bed inhomogeneities and the channeling are growing with the increasing shear thinning and linear elasticity of the liquid.

A simple two-zone fluidized bed model has been applied to the description of bed channeling. In the case of fluidization with the strongly linearly elastic liquids, the high values of the fraction f show that the main part of liquid passes through the channels. It can be concluded that the fluidized bed apparatus are unsuitable for contacting of solid particles with these liquids in the creeping flow region (e.g. for heterogeneous catalysis or bioreactors).

Symbols

d	particle diameter, m
f	fraction of the fluid volume flow rate flowing through the bed channels
F_w	corrective wall effect factor
m	Carreau flow model parameter
S	fluidized bed cross-section, m ²
S_{ch}	channel zone cross-section, m ²
u	superficial velocity, m s ⁻¹
u_B	dimensionless superficial velocity
u_{ch}	mean velocity inside channel, ms ⁻¹
u_t	particle terminal falling velocity in an unbounded liquid, ms ⁻¹
u_l	superficial velocity related to the cross-section of the zone with particles, ms ⁻¹
\dot{V}	volume flow rate, m ³ s ⁻¹
z	Richardson-Zaki exponent
$\dot{\gamma}$	shear rate, s ⁻¹
ε	mean bed voidage
ε_l	mean bed voidage of zone with particles
η	viscosity, Pa s

η_0	Carreau flow model parameter, Pas
λ	Carreau flow model parameter, s

References

- [1] Machač I., Mikulášek P., Ulbrichová I.: Chem. Eng. Sci. **48**, 2109 (1993).
- [2] Machač I., Šiška B., Lecjaks Z., Bena J.: Chem. Eng. Sci. **52**, 3409 (1997).
- [3] Machač I., Šiška B., Lecjaks Z.: Chem. Papers **53**, 390 (1999).
- [4] Teichman R., Brokl P., Šiška B., Machač I.: 15th International Congress CHISA, Prague, (2002).
- [5] Machač I., Comiti J., Brokl P., Šiška B.: TransIChemE **81**, Part A, 1217 (2003).
- [6] Šiška B., Doleček P., Bendová H., Machač I.: 16th International Congress CHISA, Prague, (2004).
- [7] Richardson J.F.: *Fluidization* (Davidson, J.F. and Harrison, D., Eds.), 25, Academic Press, New York, 1971.
- [8] Simon M.: *Study of influence of liquid rheological behavior on the structure of fluidized beds of spherical particles*, PhD thesis, University of Pardubice, 2014 (in Czech).

Figure legend

Fig. 1 Fluidized bed two-zone model

Fig. 2 Experimental setup: (1), computer; (2), video camera; (3), DC power source; (4), digital balance; (5), collecting tank; (6) fluorescent lamp; (7), milk plexiglass; (8), graphite positive electrode; (9), copper negative electrode; (10), brass grid; (11), liquid reservoir; (12), gear pump; (13), glass cooler; (14), thermostat

Fig. 3 Viscosity functions of polymer solutions used

Fig. 4 Creep and recovery tests of polymer solutions used

Fig. 5 Expansion curves for fluidization of particles P1 with polymer solutions used

Fig. 6 Structure of particle P1 beds fluidized with liquids of different rheology: (a), Tylose $u_B = 0.142$, $\varepsilon = 0.770$; (b), Natrosol $u_B = 0.157$, $\varepsilon = 0.739$; (c), Praestol $u_B = 0.278$, $\varepsilon = 0.643$; (d), Hercofloc $u_B = 0.312$, $\varepsilon = 0.614$

Fig. 7 Dependences of quantities f , ε_i , ε , and u_{ch}/u on u_B for system particle P1–solution of Tylose

Fig. 8 Dependences of quantities f , ε_i , ε , and u_{ch}/u on u_B for system particle P2–solution of Natrosol

Fig. 9 Dependences of quantities f , ε_i , ε , and u_{ch}/u on u_B for system particle P1–solution of Hercofloc

Fig. 10 Dependences of quantities f , ε_i , ε , and u_{ch}/u on u_B for system particle P2–solution of Praestol

Table 1. Characteristics of the glass spheres used

Symbol	Diameter	Density
	d (mm)	ρ (kg.m ⁻³)
P1	4.12	2594
P2	3.47	2811

Table 2. Characteristics of the test liquids, 23°C

Symbol	Liquid	Concentration (% wt.)	Density	Carreau model parameters			Rel. time
			ρ (kg.m ⁻³)	η_0 (Pa.s)	λ (s)	m (-)	λ_c (s)
L1	Tylose	1.6	1003	0.448	0.041	0.687	0.629
L2	Natrosol	0.8	1002	1.477	0.496	0.496	1.85
L3	Praestol	0.6	1002	6.690	10.011	0.390	13.6
L4	Hercofloc	0.5	1001	3.511	14.388	0.444	9.34

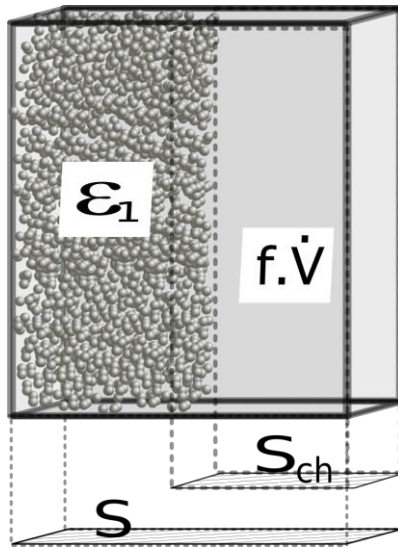


Fig. 1

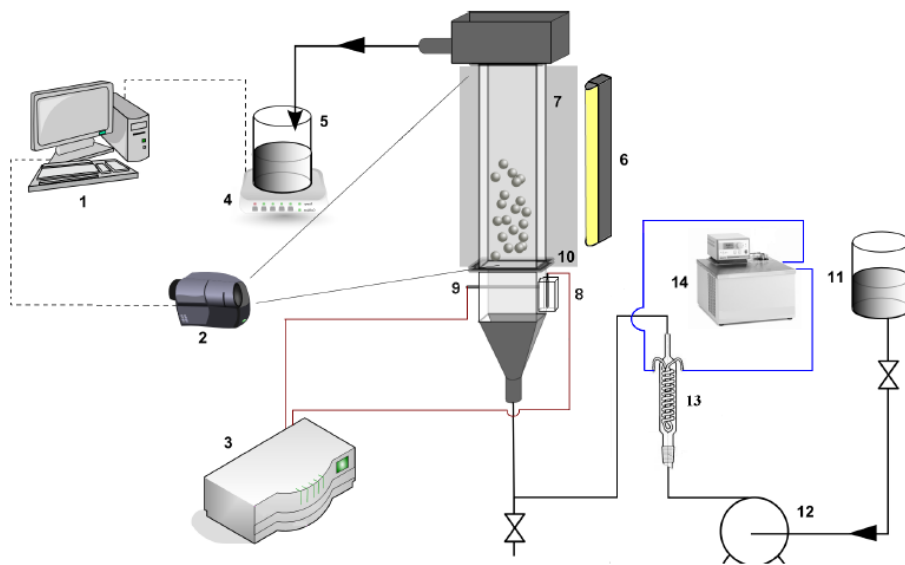


Fig. 2

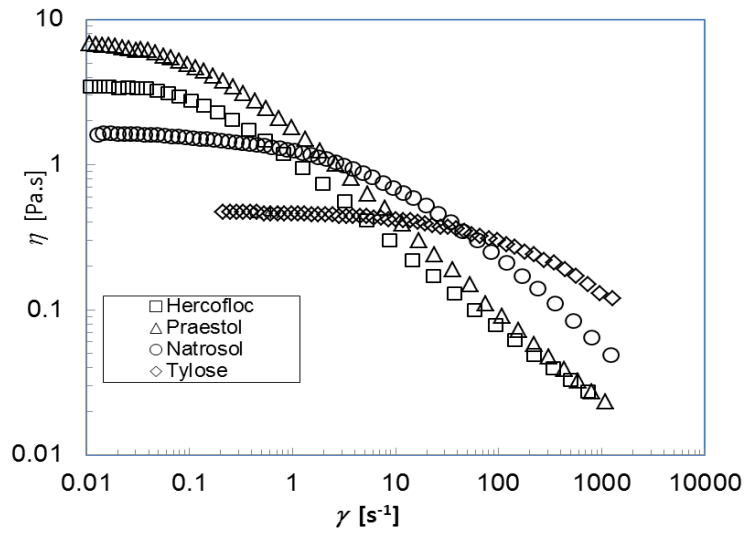


Fig. 3

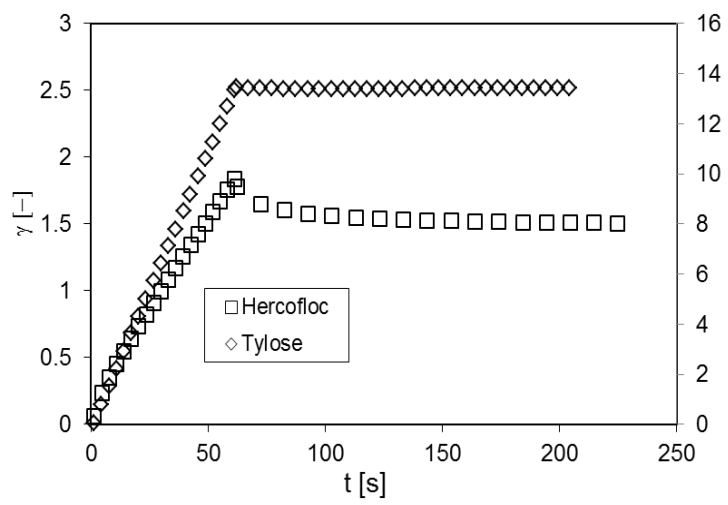


Fig. 4

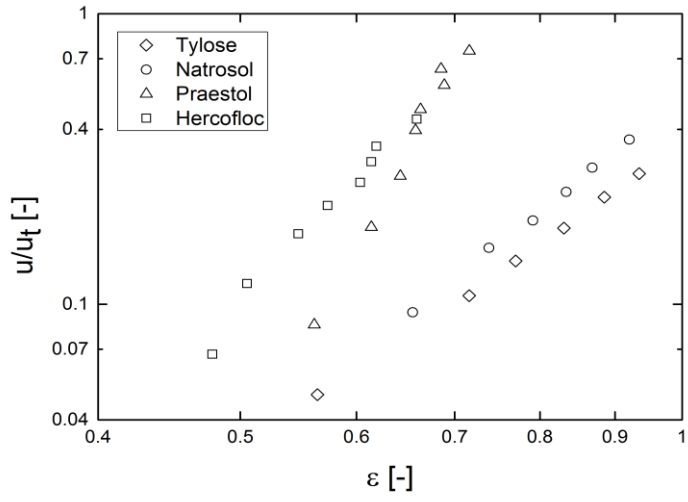


Fig. 5

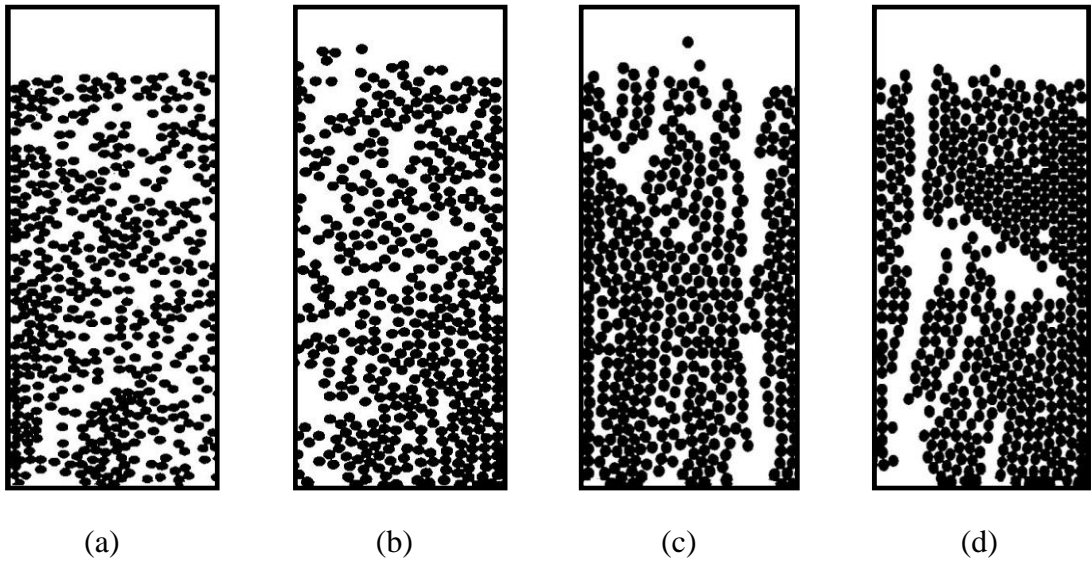


Fig. 6

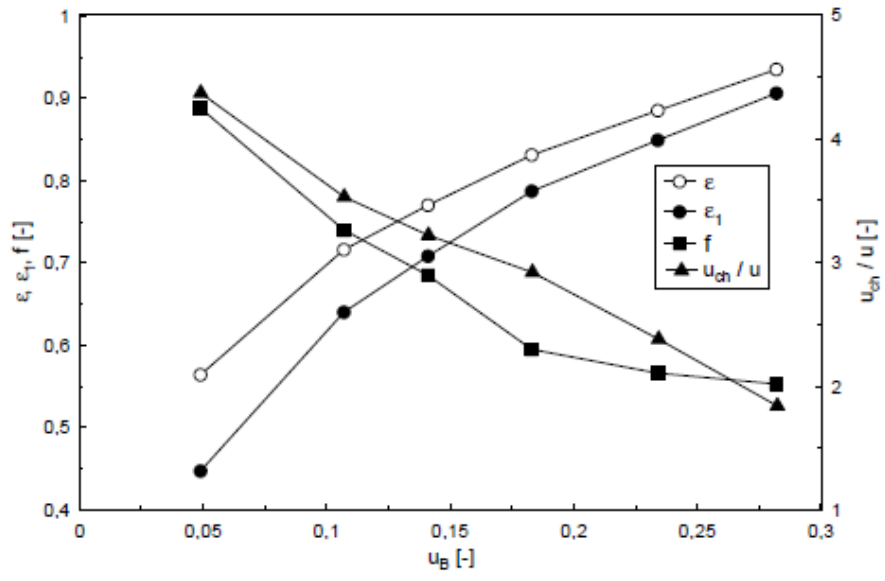


Fig. 7

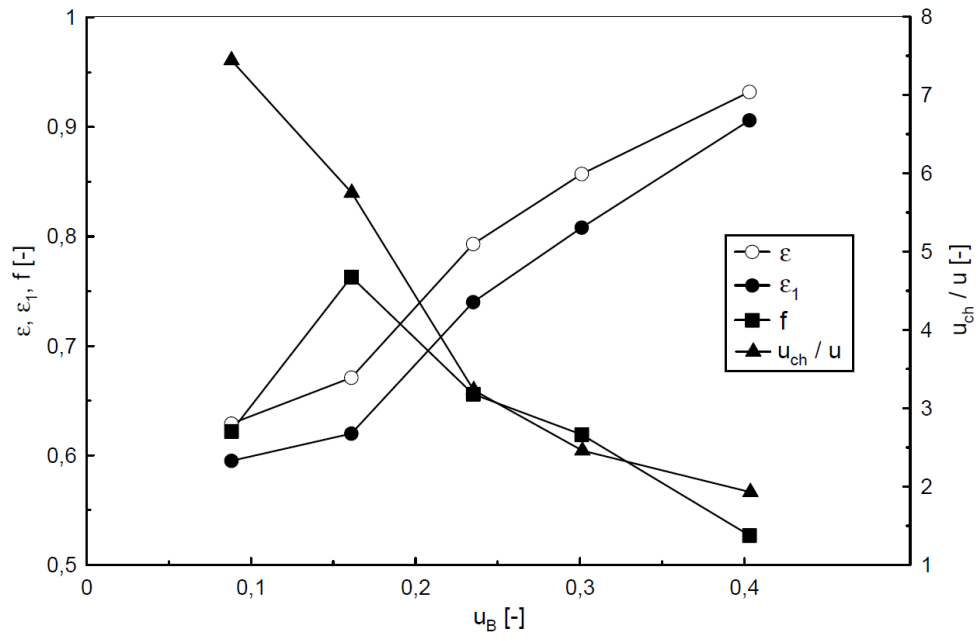


Fig. 8

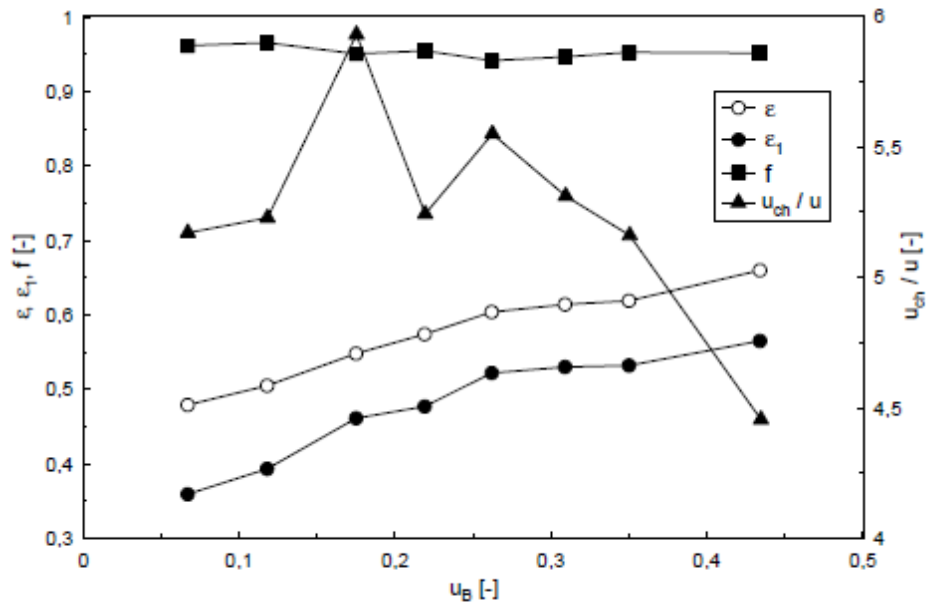


Fig. 9

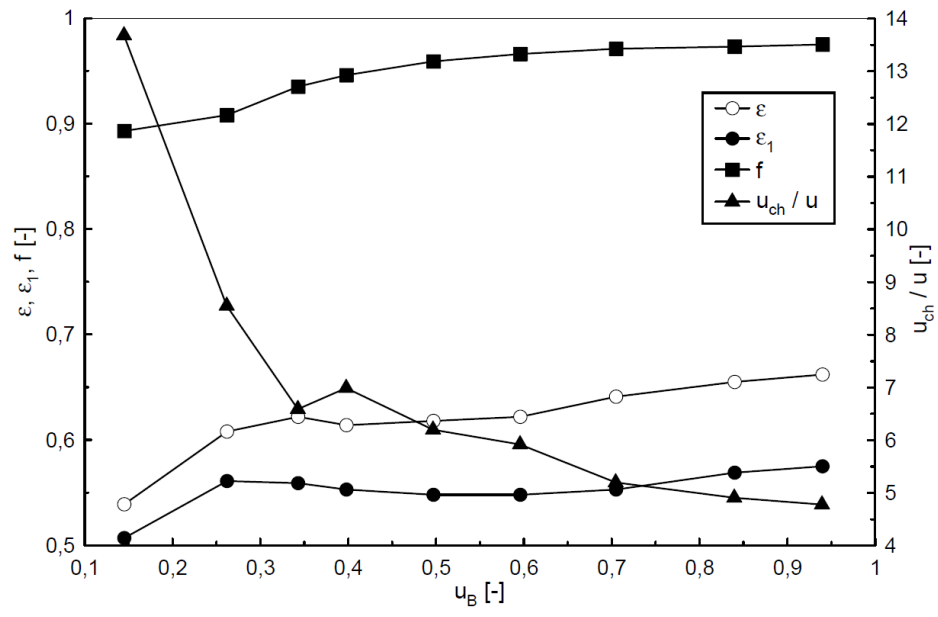


Fig. 10